Resiniferatoxin Binds to the Capsaicin Receptor (TRPV1) near the Extracellular Side of the S4 Transmembrane Domain

Margaret Z. Chou,[‡] Tecla Mtui,[‡] Ying-Duo Gao,[§] Martin Kohler,[‡] and Richard E. Middleton*[,‡]

Departments of Ion Channels and Molecular Systems, Merck Research Laboratories, Rahway, New Jersey 07065

Received November 6, 2003; Revised Manuscript Received January 7, 2004

ABSTRACT: The capsaicin receptor (TRPV1) is a nonselective cation channel that is activated in nociceptors by several painful stimuli, and hence TRPV1 antagonists could represent a novel class of analgesic compounds. Resiniferatoxin (RTX), a potent agonist of TRPV1, and iodoresiniferatoxin (I-RTX), a potent antagonist of TRPV1, both bind with higher affinity to the rat TRPV1 (rTRPV1) than the human (hTRPV1) isoform. To identify the structural features responsible for this difference in affinity, [^{3}H]RTX binding to chimeras between hTRPV1 and rTRPV1 was characterized. The "sensor" region within the transmembrane domain (S1−S4) was found to determine [^{3}H]RTX binding affinity. All 16 different residues in this region were systematically substituted in hTRPV1 with rTRPV1 residues. A single mutation in the S4 membrane domain of hTRPV1, L547M, caused a 30-fold increase in [^{3}H]RTX affinity whereas the inverse mutation in rTRPV1, M547L, caused a 30-fold decrease in affinity for [^{3}H]RTX, and several other agonists and antagonists were similarly affected by these mutations. TRPV1 channels with mutations at position 547 were expressed in oocytes, and the relative response to RTX followed a pattern similar to that seen with [^{3}H]RTX binding. These data suggest a model where Met-547 in the S4 domain of TRPV1 forms a binding pocket with Tyr-511 in the S3 domain. This model places RTX near the sensor domain thought to move during the gating process and should help to guide further work designed to understand the gating mechanisms of TRPV1 channels based on comparisons between the agonist RTX and the related competitive antagonist I-RTX.

The capsaicin receptor (TRPV1)[1] is the founding member of the TRPV family of nonselective cation channels that play a crucial role in many sensory functions (*1*−*3*). All TRP channels are structurally related to the family of six transmembrane ion channels that includes the voltage-gated cation channel family (*4*, *5*). On the basis of this homology, they are thought to be homo- or heterotetrameric proteins with a "sensor" domain formed by the first four transmembrane helices and a pore-forming domain constructed from the last two transmembrane helices (*6*, *7*). Unlike voltage-gated cation channels, TRPV channels do not contain charged residues in their fourth transmembrane domain and instead respond to physical stimuli such as changes in temperature and osmoloarity that can be modulated by second messenger systems (*1*, *8*−*10*). There is also a diverse class of phospholipid derivatives that are thought to be endogenous activators of the six identified mammalian TRPV channels as well as the larger TRP family (*11*).

TRPV1 is the most thoroughly characterized member of the TRPV family and is activated by noxious heat (>43 °C), pH <6.0, and various lipophilic compounds including capsaicin and phospholipid derivatives (*8*, *12*). It appears to be a true sensory integrator since each of the various stimuli can alter the sensitivity to other stimuli (*13*, *14*). For example, phospholipase C generated decreases in PIP_2 can increase the sensitivity to capsaicin, protons, and temperature and may explain the regulation of TRPV1 activity by several inflammatory mediators (*15*). The exogenous agonist capsaicin evidently acts via the intracellular side of the channel whereas protons activate the channel from the extracellular side (*16*−*18*). The capsaicin binding site has been partially localized to the intracellular loop between the S2 and S3 helices in the sensor domain because the efficacy of capsaicin can be modulated after mutation of either Tyr-511 or Ser-512. A model where capsaicin interacts with both the intracellular S2/S3 loop and the membrane-embedded portion of TRPV1 has been proposed (*16*).

TRPV1 plays a crucial role in pain sensation since it is activated by several painful stimuli, and mice with this gene disrupted have decreased nociceptive responses (*13*, *19*). For this reason, selective inhibitors of TRPV1 could represent novel analgesic compounds, and indeed several recent reports are consistent with this idea (*20*−*22*). However, the efficacy of the antagonist capsazepine appears to be dependent on which species is tested (*23*). To extrapolate data from animal models to humans, it is necessary to understand the source of these differences. TRPV1 is highly conserved between rat (rTRPV1) and human (hTRPV1) (87% amino acid identity); however, several pharmacological differences have

* To whom correspondence should be addressed at P.O. Box 2000, RY80N-C31, Rahway, NJ 07065. Tel: 732-594-1839. Fax: 732-594-3925. E-mail: Richard_Middleton@Merck.com.

[‡] Department of Ion Channels, Merck Research Laboratories.

[§] Department of Molecular Systems, Merck Research Laboratories.

[1] Abbreviations: DAG, diacylglycerol; I-RTX, iodo-resiniferatoxin; IP_3, inositol triphosphate; K_d, equilibrium dissociation constant; K_i, equilibrium inhibition constant; K_v, voltage-gated potassium channel; LMOD, low mode search; PIP_2, phosphatidylinositol 4,5-bisphosphate; PLC, phospholipase C; RTX, resiniferatoxin; TRP, transient receptor potential; TRPV1, transient receptor potential vanilloid type 1.

10.1021/bi035981h CCC: $27.50
Published on Web 02/10/2004

been identified (*24*, *25*). For example, resiniferatoxin (RTX), isolated from *Euphorbia resinifera*, is a more potent agonist on rTRPV1 than hTRPV1, and similar differences have been observed for the antagonist iodoresiniferatoxin (I-RTX), capsazepine, and several other vanilloid compounds (*23*, *26*−*28*). [^{3}H]RTX has proven to be a useful probe of both endogenous and heterologously expressed TRPV1 channels (*29*, *30*), and the classic vanilloid compounds, capsaicin and capsazepine, inhibit [^{3}H]RTX binding to TRPV1 in an apparently competitive manner (*31*). Finding the molecular components of this binding site may therefore provide insight into the gating mechanisms controlling TRPV1 activity.

In the present study, we have used a series of rat and human TRPV1 chimeras and single point mutations to locate the [^{3}H]RTX binding site. We have identified a single residue in the middle of the S4 transmembrane domain, 547, that appears to be responsible for many of the pharmacological differences between the rat and human isoform. Our data are consistent with a model of the TRPV1 agonist site where both agonists and antagonists interact near the pivot point in the "sensor paddle" formed from the S3/S4 transmembrane domains, and this model predicts several additional residues that potentially contribute to the binding site for RTX.

EXPERIMENTAL PROCEDURES

Materials. [^{3}H]Resiniferatoxin (43.0 Ci/mmol) was purchased from Perkin-Elmer (Boston, MA). Tinyatoxin, capsaicin, capsazepine, gingerol, sodium pyruvate, theophyline, poly(ethylenimine), and gentamycin (50 mg/mL) were purchased from Sigma-Aldrich (St. Louis, MO). All restriction enzymes were from NEN (Beverly, MA). The TsA-201 cell line, a derivative of HEK-293 cells that expresses the SV40 T antigen, was a gift of Dr. Robert DuBridge. Human dorsal root ganglia were provided by Dr. H.-G. Knaus, University of Innsbruck, Innsbruck, Austria.

TRPV1 Cloning. Rat TRPV1 in the mammalian expression vector pcDNA was kindly supplied by the laboratory of Dr. D. Julius (*12*). Human TRPV1 was cloned from a single human lumbar DRG using total RNA prepared by the Trizol method (Molecular Research Center, Cincinnati, OH). To enrich for mRNA, selection on latex oligo(dT) beads (Qiagen, Valencia, CA) was performed, and an aliquot (100 ng) was converted to cDNA using random primers according to the manufacturers' instructions (Superscript, Invitrogen). The cDNA was digested with RNase H and size selected with a Chromaspin 200 column (Clontech, Palo Alto, CA) and eluted in a final volume of 60 mL. Oligonucleotides specific for human TRPV1 were designed on the basis of the sequence of human TRPV1 (*32*) as follows: 5′-GCTAGAATTCTGAGCCACCATGAAGAAATGGAGCAGCACAGACTTGG and 3′-CGTAGCGGCCGCTATCACTTCTCCCCGGAAGCGGCAGGACTC. To facilitate the subsequent cloning steps, restriction sites were added to the primers. To amplify the TRPV1 cDNA (5 mL), the Advantage polymerase (BD Bioscience, Bedford, MA) was used in a two-step PCR protocol with the following conditions: 1 × 96 °C for 60 s, followed by 3 cycles of 95 °C for 15 s and 72 °C for 210 s and then 32 cycles of 95 °C for 15 s and 68 °C for 210 s. The resulting PCR fragment was purified with Qiagen PCR spin columns, restriction digested with *Eco*RI and *Not*I, gel purified, and resuspended in H_2O. The purified PCR fragment was ligated into the pCIneo vector (Promega, Madison, WI) prepared with the matching restriction enzymes. The ligation product was transformed in DH5α competent cells (Invitrogen). Plasmid DNA prepared from bacterial colonies was analyzed by sequencing the complete insert, and a clone whose sequence is identical to the human TRPV1 sequence previously reported was used (*32*).

Chimeras between human TRPV1 and rat TRPV1 were generated using restriction enzyme sites common to both sequences. These chimeras were made in the pBluescript vector (catalog no. 212207; Stratagene, La Jolla, CA) to minimize the impact of restriction sites also present in the larger vectors (i.e., pcDNA and pCIneo), and then *Hin*dIII/*Not*I channel inserts were transferred into the mammalian expression vector pcDNA (catalog no. V795-20; Invitrogen, Carlsbad, CA). For the N, M, and C chimeras, the common internal restriction sites used were *Bcl*I and *Xho*I (Figure 1), and the additional sites for the M1, M2, and M3 chimeras were *Bsp*HI and *Age*I (Figure 2). All constructs were verified by DNA sequencing using the BigDye terminator v3.0 cycle sequencing ready reaction and the ABI PRISM 3100 genetic analyzer (Applied Biosystems, Foster City, CA).

Point mutations were introduced into hTRPV1 using oligonucleotide-directed PCR mutagenesis. All amino acids in the M1 chimera region of hTRPV1 that were different in rTRPV1 were replaced using a two-step PCR procedure. Five point mutations, three double point mutations, and a complete replacement of the region between Asp-459 and Val-469 were done (Figure 3). The first step PCR included a mutant primer and a primer 5′ to the *Bcl*I restriction site. This resulting product was used in the second step to create a mutant DNA insert spanning the restriction sites *Bcl*I (Met-446) and *Afl*III (Lys-715). The mutant regions were sequenced in the pBluescript vector prior to digestion with *Hin*dIII/*Not*I to transfer the entire channel insert into pcDNA3. This entire insert was then sequenced again after 500−1000 μg of the pcDNA vector plus insert was produced for the transient expression experiments. The same strategy was used to generate the point mutations hTRPV1L547A and hTRPV1L547Q. A similar strategy was used to create the point mutations rTRPV1M547L, rTRPV1M547A, and rTRPV1M547Q except that the mutant insert was made between restriction sites *Sac*II (Ala-450) and *Age*I (Tyr-738).

TRPV1 Expression and Membrane Preparation. TsA-201 cells were transfected using Fugene 6 transfection reagent (catalog no. 1815075; Roche Diagnostics Corp., Indianapolis, IN), and the membranes were prepared as previously described (*28*). Briefly, cells were grown on T225 plates at a density of 5×10^6 cells/plate 24 h prior to transfection with 20 μg of plasmid DNA. Cells were fed with fresh media [DMEM/F:12 (1:1) (custom formula no. 99-0059DK) plus 10% penicillin/streptomycin (catalog no. 15070-063; Invitrogen, Carlsbad, CA) plus 10% FBS (catalog no. 100106; Gemini Bioproducts, Woodland, CA)] 24 h after transfection and harvested 54−72 h posttransfection. Cell pellets were frozen at −80 °C. Cells were lysed in 25 mM HEPES, pH 7.2 (with protease inhibitors, no. 1697498; Roche Diagnostics GmbH, Mannheim, Germany), using a 25 gauge syringe. Membrane fragments were then homogenized with a glass/glass homogenizer, the nuclei removed by centrifugation at 3000*g* for 10 min, and the remaining membranes harvested

by centrifugation at 150000*g* for 30 min. Membranes were resuspended at about 10 mg/mL in PBS (with no divalent cations) and stored at −80 °C. The protein concentration was determined using the BCA protein assay kit from Pierce (catalog no. 23227; Rockford, IL).

[^{3}H]Resiniferatoxin Binding Assays. Saturation binding curves were generated using a serial dilution approach in which the highest [^{3}H]RTX concentration (2−6 nM) was made in 5 mL membranes followed by 1:1 dilutions in the same membrane solution (2.5 mL + 2.5 mL). Membranes were diluted in binding buffer (20 mM Tris, pH 7.5, 0.01 mg/mL bacitracin) to about 5 or 50 μg/mL protein for rTRPV1 and hTRPV1 constructs, respectively. An appropriate dilution was selected empirically to ensure a significant cpm signal while maintaining the lowest possible [^{3}H]RTX binding site concentration (B_{max}), which was typically between 40 and 100 pM. It was necessary to use a new pipet after the first six dilutions in order to achieve the lowest concentrations since substantial sticking of [^{3}H]RTX to the pipet at high concentrations resulted in leaching of [^{3}H]RTX at lower concentrations. A parallel batch of membranes contained 1 μM RTX and the five highest [^{3}H]RTX concentrations (≈6−0.1 nM) to determine the linear nonspecific binding (nonspecific binding was negligible below 0.1 nM). Each dilution (2.5 mL) was incubated overnight (room temperature, in the dark), and then three 0.5 mL aliquots were filtered onto Whatman glass fiber filters (no. 1822025) pretreated with 0.5% poly(ethylenimine). The filters were then washed three times with 4 mL, 4 °C, of wash buffer (10 mM Tris, pH 7.5, 0.1% Triton X-100). The free [^{3}H]RTX was calculated by subtracting the [^{3}H]RTX bound to the filter from the total [^{3}H]RTX determined by measuring two 0.4 mL aliquots.

To measure inhibitory constants (K_i) of vanilloid ligands, membranes were diluted so that the binding site concentration was below the K_d values determined in saturation binding experiments. For example, the rTRPV1 membranes were used at a receptor site concentration of 10 pM in a total volume of 2 mL of binding buffer. This was done in order to ensure that the free inhibitor concentration was approximately the same as the total inhibitor concentration. The free [^{3}H]RTX was typically 40 pM except for rTRPV1M547L, which required about 90 pM [^{3}H]RTX to observe significant cpm. Test ligands were serially diluted at a 2× concentration and then added to 2× concentrated membranes that contained [^{3}H]RTX. Samples were incubated and filtered as described above except that the triplicate determination at each inhibitor concentration was from three separate 2 mL samples. The final concentration of RTX (and possibly the other hydrophobic test ligands) may have been overestimated since in the [^{3}H]RTX saturation experiments it was clear that a significant portion of the [^{3}H]RTX (≈10%) would stick to the pipet. RTX was apparently sticking to the plastic during the oocyte experiments described below as well.

Data Analysis. All raw data were fit using Origin 6.1 (Microcal Software, Inc., Northhampton, MA), and means, standard deviations, and Student's *t*-test analysis were calculated with Microsoft excel. A linear fit to the nonspecific binding was used to calculate the nonspecific component of the total binding at each free [^{3}H]RTX concentration, and the remainder was defined as specific binding. The specific binding was fit to a three-parameter function of the form: bound $= B_{max}/(1 + (K_d/[L])^n)$, where [L] = free [^{3}H]RTX concentration, B_{max} is the maximum specific binding, K_d is the dissociation constant, and n is the Hill coefficient. All parameters were allowed to fit freely unless the Hill coefficient fell below 1. In that case, the Hill coefficient was constrained to 1 (11 out of 106 fits).

The inhibition data for rTRPV1 and hTRPV1L547M were fit to a four-parameter function of the form: bound = max/$(1 + ([I]/IC_{50})^n)$ + nsp, where max = the maximum specific cpm bound, [I] = total inhibitor concentration, IC_{50} = inhibitor concentration at which 50% of the specific binding is inhibited, n = Hill coefficient, and nsp is the nonspecific binding. IC_{50} values were converted to K_i values using the free [^{3}H]RTX concentration, the K_d values of each channel form (Table 1), and the equation $K_i = IC_{50}/(1 + [RTX]/K_d)$.

With the binding conditions used above, it was calculated that rTRPV1 and hTRPV1L547M would have >50% of their RTX sites occupied by [^{3}H]RTX. However, due to the >10-fold lower affinity of RTX for hTRPV1 and rTRPV1M547L, these forms would have ≈10% of their total binding sites occupied. Under these conditions, there was often a stimulation of binding that reversed to inhibition at higher ligand concentrations, similar to what was reported previously (*33*). To fit these data, we used a two-binding site cooperative model of RTX binding to TRPV1 similar to what was described recently for a different ligand that binds to the K_v1.3 channel (*34*). The simplifying assumption of only two sites was necessary to restrict the number of free parameters during data fitting and does not imply that there are only two RTX sites per channel. For RTX inhibition, the equation for homotropic interaction (modified eq 11) was used: $B_E/B_{E=0} = (((\alpha K_d + [L] + [E])((\alpha K_d + [L])^2 + K_d^2(\alpha - \alpha^2)))/((\alpha K_d + [L])((\alpha K_d + [L] + [E])^2 + K_d^2(\alpha - \alpha^2))))\max) + \min$, where α = the cooperativity coefficient (when <1 stimulation is observed), K_d = the dissociation constant for RTX, [L] = free [^{3}H]RTX concentration, [E] = effector concentration, max = normalized specific binding (% control), and min = nonspecific binding. For inhibitors other than RTX, the identical equation was used except an additional dissociation constant K_e is added, K_d was not fit (i.e., values for RTX were used), and a single cooperativity coefficient (α) was used to minimize the parameters fit [modified eq 10 (*34*)]: $B_E/B_{E=0} = ((K_e(\alpha K_e K_d + [L]K_e + [E]K_d)((\alpha K_d + [L])^2 + K_d^2(\alpha - \alpha^2)))/((\alpha K_d + [L])((\alpha K_e K_d + [L]K_e + [E]K_d)^2 + K_e^2 K_d^2(\alpha - \alpha^2))))\max) + \min$. When data were fit to specific binding instead of total binding (Figures 4 and 5), the nonspecific binding (min) was forced to 0.

Oocyte Expression. Xenopus oocytes were prepared using standard techniques and incubated at 18 °C in ND-96 (96 mM NaCl, 2 mM KCl, 1 mM $MgCl_2$, 1.5 mM $CaCl_2$, 5 mM HEPES-Na, pH 7.5) that included 2.5 mM sodium pyruvate, 0.5 mM theophyline, and 50 μg/mL gentamycin. Oocytes were injected with RNA 24 h after harvesting and maintained for up to 7 days. RNA was made from the cDNA clones in pcDNA3 except for wild-type hTRPV1, which was in the pCINeo vector as described above. Plasmid DNAs were linearized with *Not*I, and RNAs were transcribed using the mMessage mMachine kit with T7 RNA polymerase (Ambion, Austin, TX). RNA was eluted in 30 μL of water, and 50 nL (≈50 ng, estimated by ethidium bromide staining of agarose gels) was injected into each oocyte.

Table 1: [^{3}H]Resiniferatoxin Binding Affinity for TRPV1 Chimeras[a]

rat TRPV1 chimeras				human TRPV1 chimeras			
channel	K_d (nM)	n_H	B_{max}	channel	K_d (nM)	n_H	B_{max}
rTRPV1-wt	0.034 ± 0.014 (n = 10)	1.51	28	hTRPV1-wt	0.44 ± 0.21 (n = 9)	1.26	1.9
rTRPV1-hN	0.022 ± 0.011 (n = 3)	1.61	6.4	hTRPV1-rN	1.19 ± 0.39 (n = 4)	1.37	8.7
rTRPV1-hM	0.52 ± 0.37 (n = 3)*	1.49	32	hTRPV1-rM	0.036 ± 0.024 (n = 3)*	1.55	7.2
rTRPV1-hC	0.031 ± 0.009 (n = 4)	1.19	12	hTRPV1-rC	0.48 ± 0.025 (n = 3)	1.21	6.7
rTRPV1-hM1	0.40 ± 0.17 (n = 4)*	1.25	26	hTRPV1-rM1	0.025 ± 0.019 (n = 4)*	1.31	3.1
rTRPV1-hM2	0.032 ± 0.011 (n = 5)	1.70	11	hTRPV1-rM2	0.39 ± 0.26 (n = 5)	1.53	3.0
rTRPV1-hM3	0.037 ± 0.014 (n = 3)	1.95	18	hTRPV1-rM3	0.48 ± 0.002 (n = 3)	1.60	2.7

[a] TRPV1 membranes expressing the indicated channels were incubated with increasing [^{3}H]RTX concentrations in the absence and presence of 1 μM RTX to define nonspecific binding. The bound [^{3}H]RTX was separated from free [^{3}H]RTX by filtration. Channel constructs were defined, and the saturation curves were fit as described in Figures 1 and 2. K_d is the average equilibrium dissociation constant (±SD), and n_H is the average Hill coefficient for the total number (n) of saturation curves determined. B_{max} values are in units of picomoles per milligram of protein. An asterisk indicates values significantly different from the corresponding wild-type control ($p < 0.01$).

TRPV1 currents were measured using a Dagan (Minneapolis, MN) two-electrode voltage-clamp amplifier (CA-1), an Instrutech (Port Washington, NY) ITC-18 computer interface, and Pulse 8.31 acquisition and analysis software (HEKA, Lambrecht, Germany). Glass microelectrodes were filled with 1 M KCl and pulled to achieve resistances of 0.5−1.0 MΩ in the bath solution. All recordings were done in ND-96(−) (ND-96 without $CaCl_2$ added) to prevent Ca^{2+}-induced inactivation of TRPV1 currents. The oocyte membrane potential was held at −50 mV, and test pulses to +50 mV were applied every 15 s during constant flow with and without drug at 3 mL/min (1 mL chamber). Only oocytes that expressed at least 1 μA of outward current at +50 mV (10 nM RTX) and had been injected at least 48 h previously were used. If oocytes were used <48 h after injection, a significant decrease in RTX sensitivity was observed. For example, in one oocyte expressing wild-type rTRPV1 for 24 h, 0.1 nM RTX only caused a response 14% as large as 10 nM RTX compared to the average of 61% for nine oocytes >48 h after injection. Two oocytes used only 48 h after injection had an average response of 30%. After 72 h, further increases in RTX sensitivity were not noted. For hTRPV1 and hTRPV1L547M channels, it was necessary to wait at least 72 h to obtain oocytes with >1 μA current, and no time-dependent changes in RTX sensitivity were observed for the next 72 h. In initial experiments, the sensitivity to RTX often increased dramatically throughout the day, but this variability was resolved when the reservoir and tubing were rinsed with ethanol between each experiment, which suggests that RTX was sticking to the plastic.

RESULTS

The S1 to S4 Transmembrane Domains of TRPV1 Determine [^{3}H]RTX Affinity. To locate the amino acid(s) responsible for the difference in RTX affinity between the rat and human TRPV1, a series of chimeric channels were constructed, and [^{3}H]RTX was used to measure its equilibrium binding properties. Membranes were prepared from TsA-201 cells after transient expression of TRPV1 channels, which was verified by western blots (see Supporting Information) and quantitated by [^{3}H]RTX saturation binding (Table 1). TRPV1 was first divided into three large segments: the amino-terminal (N), membrane spanning (M), and carboxy-terminal (C) domains, respectively (Figure 1A). Under equilibrium binding conditions, [^{3}H]RTX binds with significantly higher affinity to rTRPV1 (0.034 ± 0.014 nM, n = 10) as compared to hTRPV1 (0.44 ± 0.21 nM, n = 9; Figure 1B). Consistent with previous reports, Hill coefficients were significantly larger than 1 for both rTRPV1 and hTRPV1, suggesting multiple cooperative binding sites (Table 1). The [^{3}H]RTX potency of both the rTRPV1 and hTRPV1 chimeric channels appeared to be associated with the membrane spanning domain (M) of each channel (Figure 1C). Thus, the potency of [^{3}H]RTX for rTRPV1-hM (0.52 ± 0.37 nM) is significantly weaker than for rTRPV1-wt whereas the potency of [^{3}H]RTX for hTRPV1-rM (0.036 ± 0.024 nM) is significantly higher than hTRPV1-wt (Table 1).

To gain further insights into the residues responsible for the difference in RTX affinity, the M domain was divided into three additional regions, M1, M2, and M3 (Figure 2C). When the region that includes the first four transmembrane domains (S1−S4) from hTRPV1 was transferred to rTRPV1 (rTRPV1-hM1), the affinity for [^{3}H]RTX was significantly decreased (Figure 2B). Likewise, when the equivalent region from rTRPV1 was transferred to hTRPV1 (hTRPV1-rM1), the affinity for [^{3}H]RTX significantly increased (Figure 2B). The increased affinity for hTRPV1-rM1 (0.025 ± 0.019 nM) was the same affinity rTRPV1 has for [^{3}H]RTX, and the decreased affinity of rTRPV1-hM1 (0.40 ± 0.17 nM) was the same as wild-type hTRPV1 (Table 1). Therefore, we conclude that the amino acid(s) responsible for the difference in affinity must reside in the membrane spanning domains related to the voltage-sensing portion of voltage-gated cation channels (S1−S4) and not in the pore-forming domain (S5 and S6).

The Single Point Mutation hTRPV1L547M Explains the Species Difference in [^{3}H]RTX Affinity. Alignment of the amino acid sequences in the M1 domain identified 16 amino acid differences between rat and human TRPV1 (Figure 3A). To determine which amino acid was responsible for high-affinity binding in rTRPV1, nine PCR mutations in hTRPV1 were made. The strategy was to create a mutant protein with increased potency since this would more likely reflect a direct interaction with [^{3}H]RTX and not a nonspecific disruption of protein structure. Three of the PCR products coded for the double mutants hTRPV1M503L:T505S, hTRPV1A525V:T526S, and hTRPV1H533Q:L534R, and one was a complete change of the sequence between D459 and V469 (Figure 3A).

All nine hTRPV1 mutants expressed measurable [^{3}H]RTX binding with a similar binding site density (0.5−1.6 pmol/

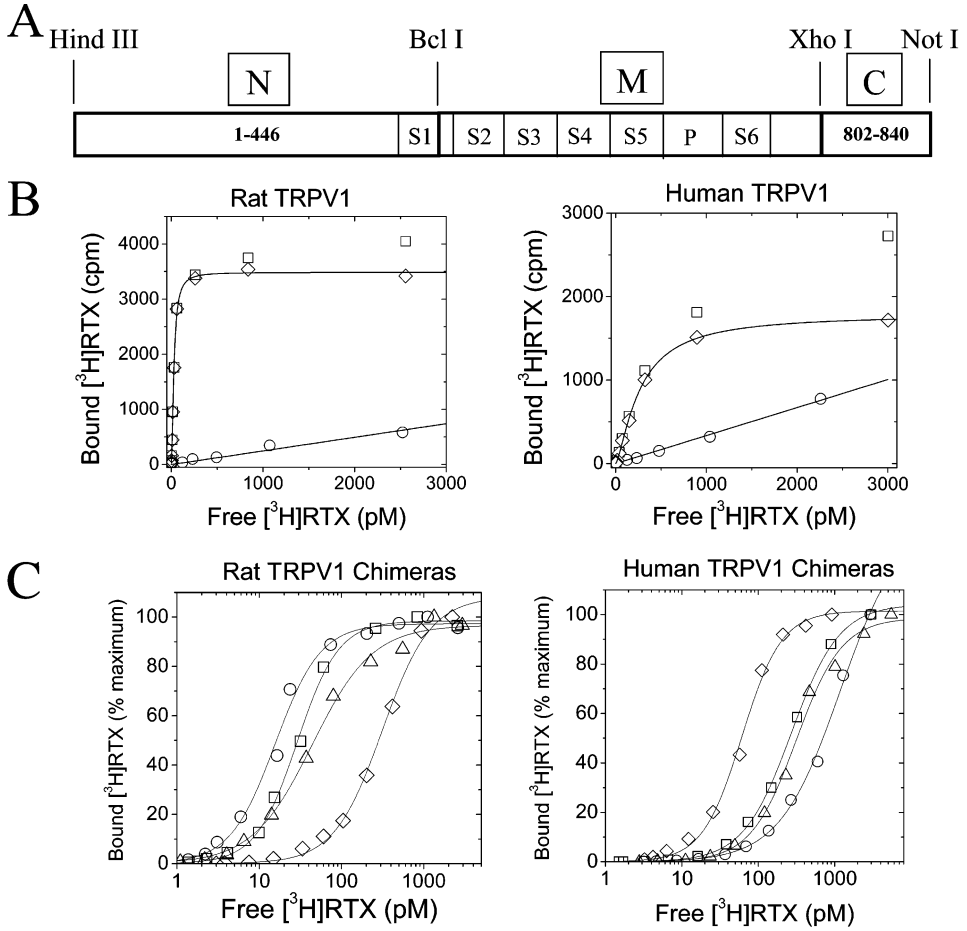

FIGURE 1: [^{3}H]Resiniferatoxin binds with high affinity to the membrane spanning domain of rat TRPV1. (A) TRPV1 was divided into three large domains, and chimeric channels were constructed for both the rTRPV1 and hTRPV1 channels using the common restriction sites indicated. N = amino terminus to Met-446, M = membrane spanning domain from Met-446 to Ala-802, and C = Ala-802 to the carboxy terminus. (B) Equilibrium binding of [^{3}H]RTX to rTRPV1 (left panel) and hTRPV1 (right panel) was measured after overnight incubation with increasing concentrations of [^{3}H]RTX in the absence and presence of 1 μM RTX. Bound [^{3}H]RTX was separated from free [^{3}H]RTX by filtration. The total (□), nonspecific (○), and specific binding (◇) at each free [^{3}H]RTX concentration tested is shown. Nonspecific binding was fit to a linear equation, and the specific binding is fit to a hyperbolic binding function where B_{max} = 3490 and 1790 cpm, K_d = 0.029 and 0.27 nM, and n_H = 1.7 and 1.4 for the rat and human TRPV1, respectively. (C) Specific binding to rTRPV1 (left panel) and hTRPV1 (right panel) chimeric channels. Wild-type rTRPV1 (□), rTRPV1hN (○), rTRPV1hC (△), and rTRPV1hM (◇) were fit to K_d values of 0.029, 0.016, 0.044, and 0.32 nM, respectively. Wild-type hTRPV1 (□), hTRPV1rN (○), hTRPV1rC (△), and hTRPV1rM (◇) were fit to K_d values of 0.27, 1.39, 0.57, and 0.061 nM, respectively.

mg of protein), and a single ≈85 kDa polypeptide was detected by western blot analysis (see Supporting Information). The equilibrium dissociation constant, K_d, for [^{3}H]RTX binding was determined for each PCR mutation and is shown in Figure 3B. Only one of the mutants, hTRPV1L547M, is different from wild-type hTRPV1, and its potency (0.015 ± 0.0026 nM, n = 6) is about 2-fold higher than that of wild-type rTRPV1 (0.034 ± 0.014 nM, n = 10). When the reverse mutation was made in rTRPV1, M547L, [^{3}H]RTX affinity was substantially reduced to 1.12 ± 0.32 nM (n = 6), a value that reflects a lower affinity than wild-type hTRPV1 (0.44 ± 0.21 nM, n = 9; Figure 3C).

In an attempt to understand why Met-547 confers higher affinity for RTX than Leu-547, the small side-chain alanine (rTRPV1M547A and hTRPVL547A) and the hydrophilic side-chain glutamine (rTRPV1M547Q, and hTRPV1L547Q) were also put at position 547. Though grossly different in side-chain chemistry, both mutations reduced binding affinity of [^{3}H]RTX for rTRPV1, but the rTRPV1M547Q caused a slightly less dramatic shift in potency than rTRPV1M547A (Figure 3C, 7-fold vs 36-fold, respectively). Surprisingly, neither mutation caused a bigger decrease in potency than the more conservative substitution M547L. When substituting these residues in hTRPV1, no measurable [^{3}H]RTX binding was detected, but a similar amount of protein was observed on western blots (see Supporting Information). Due to nonspecific binding levels, [^{3}H]RTX specific binding is difficult to detect above 5 nM (Figure 1B), but a shift in potency for hTRPV1 of <10-fold would have been detected, and therefore a >10-fold shift in affinity must have occurred. Apparently there are other differences in the RTX binding site between the human and rat TRPV1 not accounted for by position 547 alone since binding is detectable for the corresponding rTRPV1 M547Q and M547A mutants.

Other Ligands Also Show Differences in Potency That Depend on the Residue at Position 547. To better understand the molecular pharmacology of the RTX binding site, several agonists were examined for differences between rTRPV1 and hTRPV1 (Figure 4). Assay conditions were chosen to maintain the same free [^{3}H]RTX concentration (≈40 pM) for all channel forms, and therefore, the lower affinity forms had substantially reduced receptor site occupancy compared

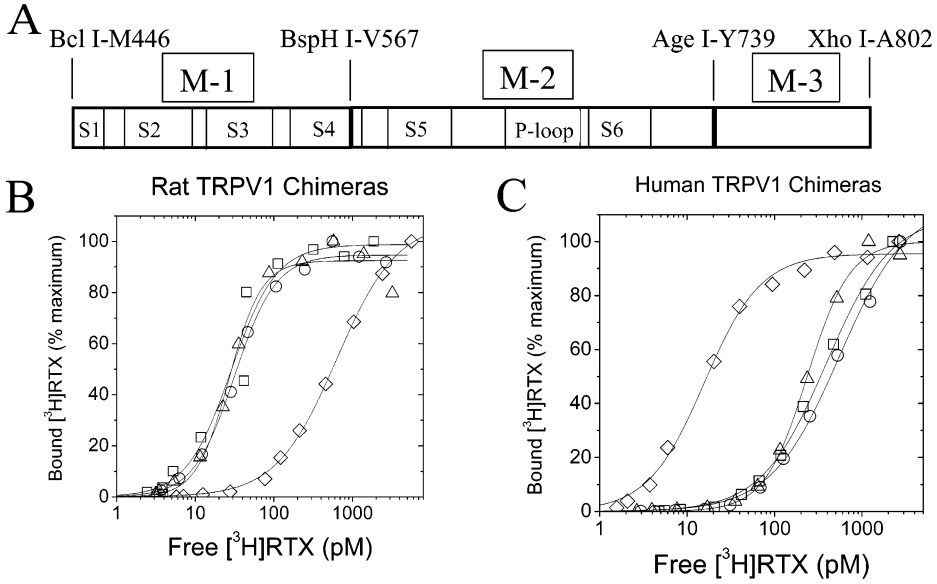

FIGURE 2: High-affinity [^{3}H]resiniferatoxin binding is located within the S1 to S4 transmembrane domains of rat TRPV1. (A) The transmembrane domain (M) was further divided into three parts using the common restriction sites *Bcl*I, *Bsp*HI, *Age*I, and *Xho*I. The M1 region spanned from Met-446 to Val-567, the M2 region spanned from Val-567 to Tyr-739, and the M3 region spanned from Tyr-739 to Ala-802. (B) Specific [^{3}H]RTX binding to wild-type rTRPV1 (□), rTRPV1-hM1 (◇), rTRPV1-hM2 (○), and rTRPV1-hM3 (△) was fit to K_d values of 0.029, 0.63, 0.032, and 0.027 nM, respectively. (C) Specific [^{3}H]RTX binding to wild-type hTRPV1 (□), hTRPV1-rM1 (◇), hTRPV1-rM2 (○), and hTRPV1-rM3 (△) was fit to K_d values of 0.39, 0.016, 0.55, and 0.24 nM, respectively.

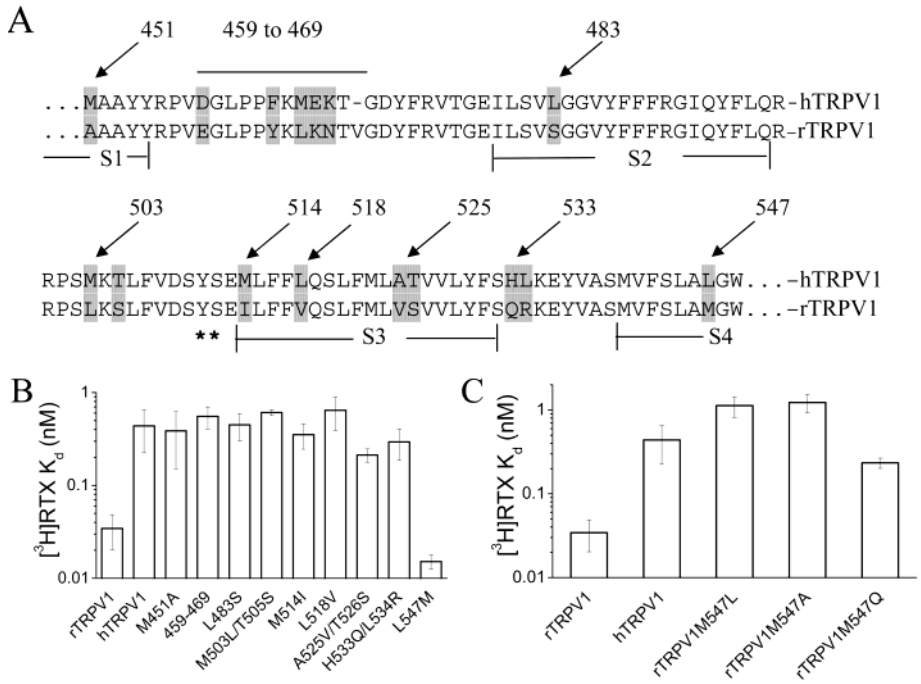

FIGURE 3: The amino acid at position 547 controls [^{3}H]RTX affinity. (A) Amino acid sequences from the M1 region of rTRPV1 and hTRPV1 are aligned, and the differences are highlighted. Arrows show each individual point mutation made in hTRPV1 and for 503, 525, and 533 the first residue of two changes made simultaneously. The region between 459 and 469 was changed to the rat sequence in one construct. Asterisks mark the residues previously identified as important for capsaicin activity (*16*). The putative membrane spanning regions defined by hydrophobic analysis (S1, S2, S3, and S4) are also shown (*12*). (B) The mean and standard deviation of the K_d's determined for each mutated channel ($n = 3-6$) from data fits as described in Figure 1 and Experimental Procedures. (C) The mean and standard deviation of the K_d's determined for point mutations made at position 547 in rTRPV1 ($n = 3-6$).

to the higher affinity forms. As a result, low concentrations of RTX actually stimulated binding to the low-affinity hTRPV1-wt and rTRPV1M547L forms, and at higher concentrations inhibition was observed (Figure 4A). This result is consistent with cooperative binding to multiple identical sites on a protein, and the data were fit with a function based on this type of model (see Experimental Procedures). The calculated K_i's are generally 3−5-fold larger than the corresponding K_d values determined above, but the relative potencies are very similar (Table 2). This apparent shift in potency may be due to RTX sticking to plastic surfaces (see Experimental Procedures). The agonist tinyatoxin is a close analogue of resiniferatoxin in which the methoxy group of the vanilloid ring has been removed

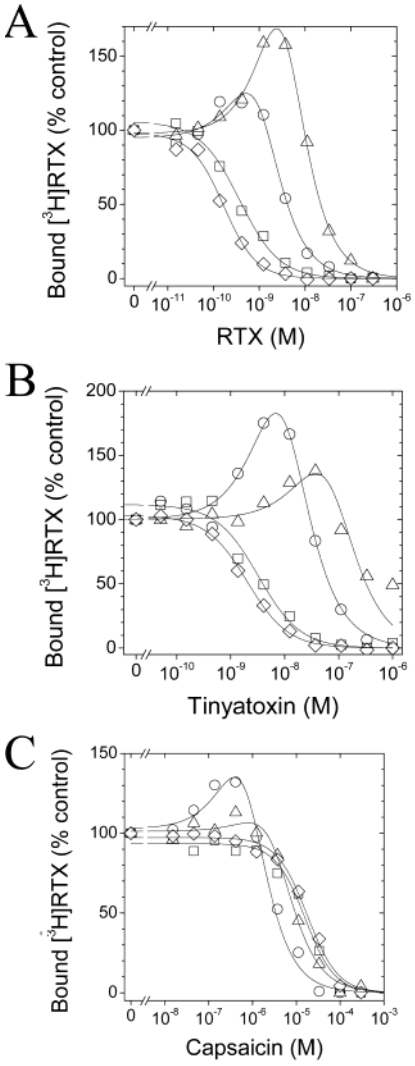

FIGURE 4: The amino acid at position 547 explains species differences in agonist binding. The indicated TRPV1 channel was incubated overnight with [^{3}H]RTX and the indicated concentration of inhibitor. Samples were filtered, and the bound [^{3}H]RTX was measured. Specific binding was calculated by subtracting the bound [^{3}H]RTX at the highest inhibitor concentration, and the data were normalized to the [^{3}H]RTX bound in the absence of inhibitor. If the test ligand did not completely inhibit all specific binding (weak inhibition), nonspecific binding was determined by another inhibitor. Data for rTRPV1 (□) and hTRPV1L547M (◇) were fit to three-parameter inhibition curves with IC_{50} = 0.36 and 0.17 nM, respectively, for RTX (A), IC_{50} = 3.1 and 2.1 nM, respectively, for tinyatoxin (B), and IC_{50} = 18000 and 21000 nM, respectively, for capsaicin (C). Data for hTRPV1 and rTRPV1M547L were fit to a function that accounted for positive cooperativity (see Experimental Procedures) and, hence, allowed for increased binding at low inhibitor concentrations. The calculated dissociation constants for hTRPV1 (○) and rTRPV1M547L (△) were 2.55 and 12.2 nM, respectively, for RTX (A), 36 and 160 nM, respectively, for tinyatoxin (B), and 1800 and 6300 nM, respectively, for capsaicin (C).

(*35*). It was also tested for its ability to inhibit [^{3}H]RTX binding to the four channel types to determine if this modification affected the interaction with the 547 position (Figure 4B). Again a pronounced stimulation was observed at low tinyatoxin concentrations. The rTRPV1 bound tinyatoxin (K_i = 1.1 ± 0.6 nM, n = 3) nearly 50-fold more potently than hTRPV1 (K_i = 210 ± 81 nM, n = 3) but with similar potency to hTRPV1L547M (K_i = 0.43 ± 0.11 nM, n = 3). No difference in the potency of capsaicin for any of these channel forms was observed (Figure 4C, Table 2), and no difference in the potency of the related agonist gingerol was found (data not shown).

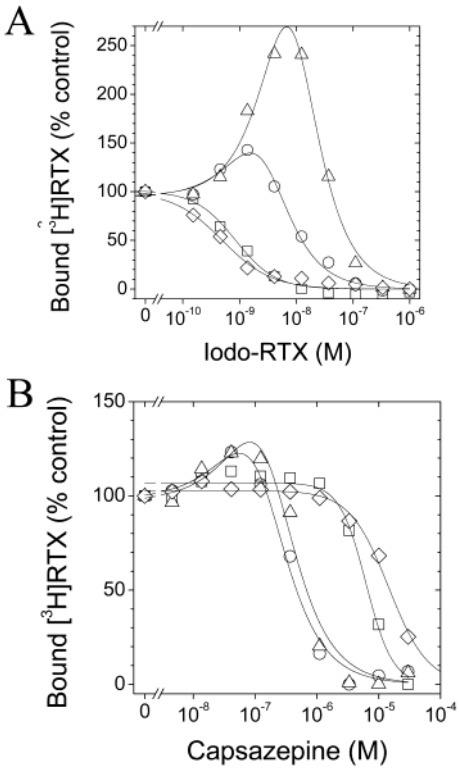

FIGURE 5: The amino acid at position 547 explains species differences in antagonist binding. Experiments were done and data plotted as in Figure 4. Data for rTRPV1 (□) and hTRPVL547M (◇) were fit with IC_{50} = 0.93 and 0.44 nM, respectively, for I-RTX (A) and IC_{50} = 6800 and 14000 nM, respectively, for capsazepine (B). The calculated dissociation constants for hTRPV1 (○) and rTRPV1M547L (△) were 7.3 and 46 nM, respectively, for I-RTX (A) and 280 and 423 nM, respectively, for capsazepine (B).

To further substantiate a direct binding interaction between the 547 residue in S4 and vanilloid ligands, two competitive antagonists were also examined. I-RTX is a halogenated version of RTX that has no agonist activity but retains nearly the same potency as RTX. I-RTX shows the same difference in potency between rTRPV1 and hTRPV1, and the nature of the residue at position 547 determines its potency (Figure 5A). In addition, a similar stimulation in binding at low I-RTX concentrations to hTRPV1 and rTRPV1M547L was observed. These data indicate that both the cooperative nature of binding and the effect of residue 547 on binding affinity are not exclusive to agonist action on TRPV1. Finally, the antagonist capsazepine, unlike the RTX-like structures, or capsaicin binds more potently to hTRPV1 (K_i = 207 ± 47 nM, n = 3) than rTRPV1 (K_i = 3300 ± 130 nM, n = 3) but does not seem to stimulate binding (Figure 5B, Table 2). However, the K_i values for inhibition of [^{3}H]RTX binding to both hTRPVlL547M (4100 ± 900 nM, n = 3) and rTRPV1M547L (560 ± 150 nM, n = 3) indicate that residue 547 appears to be at least partially responsible for the difference in affinity. Therefore, the 547 residue is also part of the capsazepine binding site in TRPV1.

Functional Characterization of Mutants at Position 547. To determine if the nature of the residue at position 547 in TRPV1 also alters the relative response to RTX as a functional agonist of the channel, rTRPV1, hTRPV1, and

Table 2: Potency (K_i) of Several Vanilloid Ligands on rTRPV1, hTRPV1, and Position 547 Mutants[a]

channel	RTX	tinyatoxin	capsaicin	I-RTX	capsazepine
rTRPV1-wt	0.17 ± 0.008	1.08 ± 0.59	7510 ± 840	0.64 ± 0.18	3310 ± 130
rTRPV1-M547L	12.0 ± 0.15*	217 ± 100*	5476 ± 1110	72 ± 17*	654 ± 200*
hTRPV1-wt	2.6 ± 0.39	61 ± 15	1950 ± 400	10.4 ± 2.9	237 ± 55
hTRPV1-L547M	0.041 ± 0.004*	0.43 ± 0.11*	5770 ± 1300	0.13 ± 0.02*	4070 ± 940*

[a] TRPV1 membranes expressing the indicated channels were incubated with [^{3}H]RTX and increasing concentrations of the indicated inhibitor as described in Figure 4. An asterisk indicates values significantly different from the corresponding wild-type control ($p < 0.01$). K_i values (nM) are presented as the mean ± SD ($n = 3$ or 4) derived from four-parameter inhibition curves as described in Experimental Procedures.

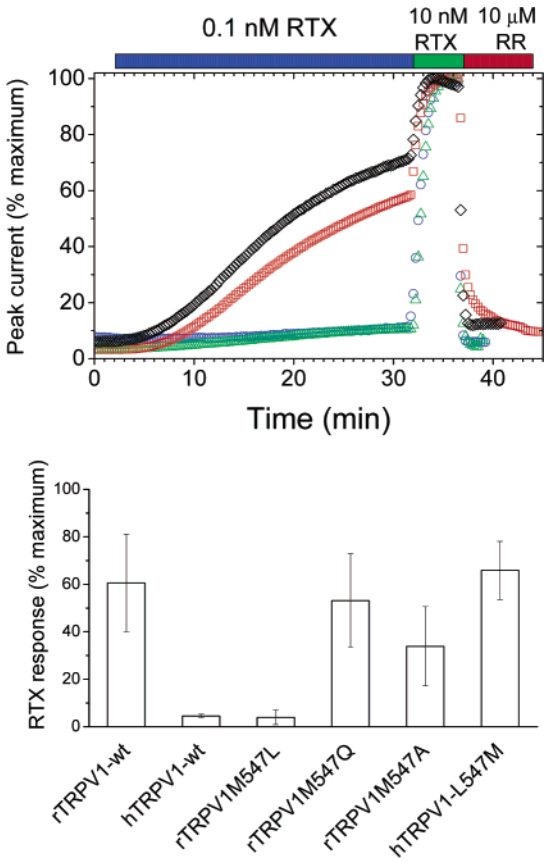

FIGURE 6: Functional expression and RTX sensitivity of mutations at position 547. Top panel: RNA encoding rTRPV1 (red, □), hTRPV1 (blue, ○), rTRPV1M547L (green, △), and hTRPV1L547M (black, ◇) channels was synthesized and injected into *Xenopus* oocytes. After at least 48 h, oocytes were voltage-clamped at −50 mV, and outward currents were measured every 15 s at +50 mV. After 2 min, 0.1 nM RTX was added for 30 min, followed by 10 nM RTX for 5 min to define maximum RTX response. To determine how much of the outward current was due to RTX activation of TRPV1, the noncompetitive TRPV1 inhibitor ruthenium red (10 μM) was applied for 5 min. Bottom panel: The response to RTX was determined after subtraction of the leak current (current not blocked by ruthenium red). Response to 0.1 nM RTX was defined as the outward current obtained after 30 min in 0.1 nM RTX divided by the response to 10 nM RTX and expressed as percent maximum response. Comparison of the relative response of 0.1 nM RTX revealed that rTRPV1 had 61 ± 20% ($n = 9$), hTRPV1 had 4.6 ± 0.7% ($n = 6$), rTRPV1M547L had 3.9 ± 3.0% ($n = 6$), hTRPV1L547M had 66 ± 12% ($n = 6$), rTRPV1M547Q had 53 ± 20% ($n = 6$), and rTRPV1M547A had 34 ± 17% ($n = 8$) the response of 10 nM RTX.

several 547 mutants were expressed in oocytes and challenged with RTX (Figure 6). Oocytes were voltage-clamped at −50 mV, and outward currents were measured at +50 mV. All tests were done in the absence of calcium in order to obtain stable responses. When 10 nM RTX was used to define maximum response, a stable response that lasted at least 5 min was typically observed. Application of 0.1 nM RTX to rTRPV1 for 30 min caused a slow increase in outward current (Figure 6, squares). The 30 min application period was determined by extrapolation from preliminary tests at 0.2 and 0.5 nM RTX where a clear peak response was observed after 15 and 7 min, respectively (data not shown). Longer incubation times were problematic since many oocytes acquired a substantial amount of leak current during the 45 min experiment. Maximum TRPV1 outward current was defined as the current elicited by a 5 min application of 10 nM RTX. To determine how much of the 10 nM RTX response was from TRPV1 and not leak current, 10 μM ruthenium red was applied. Data from oocytes in which at least 90% of the maximal response was blocked by ruthenium red were used. In some batches, very few oocytes passed these criteria due to substantial leak accumulation over the 45 min experiment.

In this experimental protocol, 0.1 nM RTX was clearly less potent on hTRPV1 (circles) than rTRPV1 (squares, Figure 6). However, when the mutant hTRPV1L547M was tested (diamonds), a response very similar to wild-type rTRPV1 was observed. In contrast, the mutant rTRPV1M547L (triangles) barely responded to 0.1 nM RTX. Quantitation of the response relative to 10 nM RTX showed that 0.1 nM RTX activated rTRPV1 61 ± 21% ($n = 9$) of maximum whereas it activated hTRPV1 4.6 ± 0.7% ($n = 6$) of maximum (Figure 6B). The mutant hTRPV1L547M was more sensitive to 0.1 nM RTX with a relative response of 66 ± 12% ($n = 6$), and conversely the mutant rTRPV1 channel M547L barely responded to 0.1 nM RTX (3.9 ± 3.0%, $n = 6$). The response from the other rTRPV1 mutants, M547Q (53 ± 20%, $n = 6$) and M547A (34 ± 17%, $n = 8$), was closer to wild-type rTRPV1 than hTRPV1. The hTRPV1L547Q mutant responded to 10 nM RTX, pH 5.0, and capsaicin, but the maximum expression level (315 ± 245 nA, $n = 4$) was too low to quantitate the RTX response. Furthermore, oocytes expressing the hTRPV1L547A mutant did not respond to RTX, capsaicin, or pH 5.0, indicating that hTRPV1 is less tolerant to substitutions at position 547 than rTRPV1.

DISCUSSION

The goal of this study was to identify the molecular basis for the 10-fold difference in RTX affinity between the rat and human TRPV1. By preparing a series of rat/human chimeric TRPV1 channels, the region that contains the S1 to S4 transmembrane domains was determined to be responsible for conferring high-affinity [^{3}H]RTX binding to rTRPV1. Systematic replacement of the amino acids in this domain of hTRPV1 with the corresponding rTRPV1 residues identified a single conservative substitution of methionine

for leucine at position 547 in the S4 domain that accounted for the species difference in RTX binding. The amino acid at this position also affected the potency of the antagonists I-RTX and capsazepine for inhibiting [^{3}H]RTX binding and the agonist response to RTX. These results clearly implicate a role for the S4 domain in the gating of TRPV1, similar to the role it plays in the structurally related voltage-gated cation channel family.

One of the most striking results from the present study is that the conservative substitution of leucine for methionine can result in a 30-fold shift in RTX potency. This modest chemical change affects both agonists and competitive antagonists and can both increase and decrease binding affinity. Although the sulfur atom in methionine can participate in weak hydrogen bonds and other chemical interactions (*36*, *37*), it is also possible that the methionine could participate in steric or hydrophobic interactions with RTX. The M547A mutation in rTRPV1 reduces RTX affinity to the same degree as M547L (≈30-fold) and suggests that, at least in the rat isoform, leucine contributes very little to RTX equilibrium binding affinity. A more radical mutation, M547Q, decreased potency to a smaller degree than either M547A or M547L and may indicate that methionine and glutamine contribute some positive binding energy with RTX since they can extend farther from the backbone. However, in a functional assay, both the M547A and M547Q mutations caused less of a detrimental affect on RTX agonist activity than M547L, which indicates that there is some difference between RTX equilibrium binding and channel activation. The L547A and L547Q mutations in the hTRPV1 were less informative since no [^{3}H]RTX binding and little channel activity were detected even though protein was seen on western blots. However, this result indicates that the simple-minded picture that the residue at position 547 is the only relevant difference between rTRPV1 and hTRPV1 is not correct since rTRPV1M547A and rTRPV1M547Q had different properties than hTRPV1L547A and hTRPV1L547Q, respectively. In fact, the observation that the human L547M mutation has a higher affinity for RTX than wild-type rTRPV1 (Figures 3 and 4), and similarly that the rat M547L displays a lower affinity than wild-type hTRPV1, also suggests that other amino acid differences are important.

Capsaicin, I-RTX, and capsazepine are all thought to bind to the same site(s) on the TRPV1 channel as RTX and, hence, are expected to interact with the same portion of the S4 transmembrane domain (*20*, *31*, *38*). It seems likely that there are four identical binding sites in each channel, one within the sensor domain of each subunit of the homotetramer. This model is consistent with recent single-channel analysis of capsaicin-stimulated TRPV1 that shows multiple burst durations that depend on the concentration of capsaicin, as if increasing the number of bound capsaicin molecules shifts the channel incrementally to longer burst durations (*39*). Previously, it was thought that capsaicin binds to the intracellular side of TRPV1 since a membrane-impermeant analogue of capsaicin could only activate the channel from the intracellular side (*18*). Furthermore, two residues located in the S2−S3 intracellular loop (Tyr-511, Ser-512) were found to be critical for both capsaicin activation and RTX binding to TRPV1 channels (*16*). These results led to a model for the capsaicin binding site where the vanilloid group interacts with Tyr-511 on the intracellular side of each subunit within the channel and the hydrophobic tail protrudes into the membrane. Our results extend this model by identifying a region in the membrane domain with which capsaicin may interact.

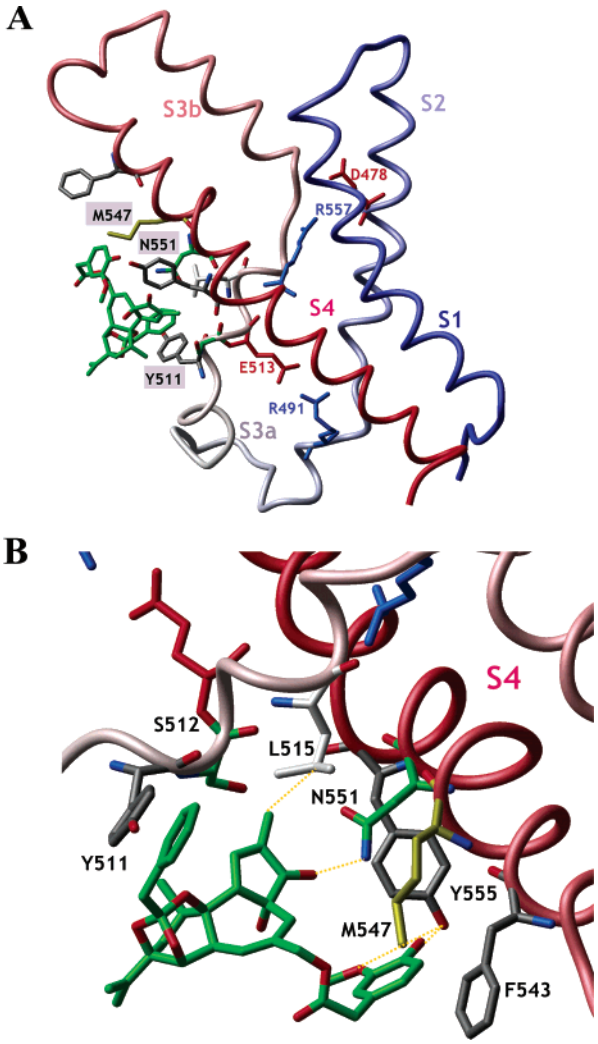

FIGURE 7: Hypothetical model of the RTX binding site in hTRPV1. (A) Docking model of RTX with a homology model of hTRPV1L547M. The homology model was generated using the structure of the isolated voltage-sensor domain from K_vAP as a template (*6*, *7*) and the molecular operating environment (MOE), version 2002.03, software (Chemical Computing Group Inc., Montreal, Canada). The structure is oriented so that the S1−S2 and S3b−S4 connecting loops are at the top and the S2−S3a connecting loop is at the bottom as if they were located on the extracellular and intracellular side of the membrane, respectively. The docking was performed using the LMOD method, which allows residue side chains within 5 Å proximity of the ligand to be flexible (*47*). The side chains around the potential RTX binding site, Y511, S512, L515, F543, M547, N551, Y555, and two potential ionic bonds (E513:R491, D478:R557) are shown. The aromatic side chains are colored in gray, nonpolar in white, Met in yellow, and polar in green; negatively charged residues are in red, and positively charged residues are in blue. Panel B presents a more detailed view of the RTX docking model from a different angle so close contacts can be seen.

To get some insight into the structure of the binding site, we generated a homology model for the sensor domain of hTRPV1 (S1−S4) based on the crystal structure of the equivalent domain of K_vAP (*7*; Figure 7). One of the features of this hypothetical model is the placement of the 547 side chain near Tyr-511 and Ser-512. These residues are critical

for capsaicin sensitivity and, in the model, form a pocket in which RTX can fit. The binding pocket shown is wedged between the flexible S3 region and the "voltage"-sensor paddle using the extended conformation of S4 that supposedly represents the open state (*40*). If the S4 were to move into the closed, bent conformation, this binding pocket could then collapse. This model also predicts contributions of Leu-515, Phe-543, Asn-551, and Tyr-555 to the binding of RTX in order to be consistent with previous structure−activity relationships for RTX (*41*, *42*). The methoxy group at the 3-position in the vanilloid ring is shown as a weak bond to Tyr-555, consistent with the ≈5-fold decrease in potency for tinyatoxin which lacks this group [Table 2 (*35*)]. When modeling capsaicin into this pocket (data not shown), the vanilloid headgroup interacts with Tyr-511 as previously suggested (*16*). Interestingly, the structure−activity relationship for the vanilloid ring in capsaicin is substantially different than for RTX, and the difference could be explained by the model presented here where the vanilloid of RTX interacts with Tyr-555 instead of Tyr-511 (*42*−*44*). If the traditional structural model is used instead of the K_vAP crystal structure, the sensor domain would then be constructed from antiparallel α helices that are arranged perpendicular to the membrane plane. In this case, the 547 and 511 residues would be about 20 Å apart, a distance greater than the 16 Å length predicted for RTX. Of course, it is possible with modest changes in domain alignment and the added dimension of side-chain flexibility that a classic S1−S4 α-helical model could accommodate RTX.

One of the most intriguing properties of TRPV1 channels is their ability to respond in a graded fashion to several stimuli simultaneously. Presumably, the different stimuli eventually lead to opening of a common channel gate. Protons apparently activate the channel by binding to extracellular amino acids near the pore domain, and mutation of these negatively charged residues can also affect the capsaicin sensitivity (*17*, *45*). In contrast, mutation of conserved residues in the pore-forming region of S6 can differentially affect capsaicin and proton sensitivity with relatively little effect on [^{3}H]RTX binding (*46*), which suggests that the capsaicin and proton binding sites are physically separated. It is possible that the various stimuli can converge within the membrane to control the movement of the sensor paddle, which evidently can move from the inside to the outside of the cell. On the basis of homology to K_v channels, the final gating event would then involve movement of the intracellular portion of the S6 transmembrane helix (*40*).

In addition to structurally defining the agonist binding site, it is also necessary to understand how binding can translate into opening of the channel. Interestingly, I-RTX, a monoiodination of the vanilloid ring of RTX, is equipotent to RTX but completely loses its agonist activity (*20*, *28*), and similar effects have been reported after halogenation of a capsaicin analogue (*44*). I-RTX inhibits the activation of TRPV1 by both capsaicin and RTX in an apparently competitive manner (*38*). Increasing concentrations of I-RTX, like RTX itself, cause a stimulation of [^{3}H]RTX binding at low concentrations followed by complete block at higher concentrations. Evidently, I-RTX can cause the same allosteric modification of the [^{3}H]RTX binding site as RTX even though it does not open the channel. One possible explanation for these results is that binding of either agonists or antagonists initiates movement of the sensor paddle, but only agonists and partial agonists allow subsequent rearrangement of the S5/S6 intracellular region to open the channel.

It is still unclear what, if any, endogenous ligand(s) substitute(s) for RTX and capsaicin to activate TRPV1 physiologically. PLC can sensitize TRPV1 to capsaicin and heat stimuli by cleaving PIP_2 into DAG and IP_3 (*15*). The PIP_2 binding site is located in the carboxy-terminal domain some distance from the putative capsaicin binding site within the sensor domain. It is tempting to imagine that the DAG portion of PIP_2 could compete with capsaicin (or RTX) for binding to the S3−S4 sensor paddle since several phospholipid derivatives are thought to be endogenous activators of TRPV1 and other TRP channels (*11*). Though these two portions of the channel are separated in linear protein sequence, they may be very close in the actual folded TRPV1 structure. If so, PIP_2 may inhibit channel activity by anchoring the sensor paddle bound to its DAG portion to the intracellular carboxy-terminal domain that interacts with the PIP_2 phosphate headgroup. This model would predict that residues in the S3/S4 region would affect both capsaicin and PIP_2 activity, and additional point mutations in this region could help to further elucidate the connection between the various TRPV1 stimuli.

ACKNOWLEDGMENT

We thank Drs. Gregory Kaczorowski and Maria Garcia for critical review and editing of the manuscript.

SUPPORTING INFORMATION AVAILABLE

Western blots showing the relative amount of protein expressed from each of the constructs discussed in this paper. This material is available free of charge via the Internet at http://pubs.acs.org.

REFERENCES

1. Montell, C., Birnbaumer, L., and Flockerzi, V. (2002) The TRP channels, a remarkably functional family, *Cell 108*, 595−598.
2. Birnbaumer, L., Yidirim, E., and Abramowitz, J. (2003) A comparison of the genes coding for canonical TRP channels and their M, V and P relatives, *Cell Calcium 33*, 419−432.
3. Gunthorpe, M. J., Benham, C. D., Randall, A., and Davis, J. B. (2002) The diversity in the vanilloid (TRPV) receptor family of ion channels, *Trends Pharmacol. Sci. 23*, 183−191.
4. Yellen, G. (2002) The voltage-gated potassium channels and their relatives, *Nature 419*, 35−42.
5. Clapham, D. E., Runnels, L. W., and Strubing, C. (2001) The TRP ion channel family, *Nat. Rev. Neurosci. 2*, 387−396.
6. Doyle, D. A., Morais Cabral, J., Pfuetzner, R. A., Kuo, A., Gulbis, J. M., Cohen, S. L., Chait, B. T., and MacKinnon, R. (1998) The structure of the potassium channel: Molecular basis of K^+ conduction and selectivity, *Science 280*, 69−77.
7. Jiang, Y., Lee, A., Chen, J., Ruta, V., Cadene, M., Chait, B. T., and MacKinnon, R. (2003) X-ray structure of a voltage-dependent K^+ channel, *Nature 423*, 33−41.
8. Szallasi, A., and Blumberg, P. M. (1999) Vanilloid (capsaicin) receptors and mechanisms, *Pharmacol. Rev. 51*, 159−212.
9. McKemy, D. D., Neuhausser, W. M., and Julius, D. (2002) Identification of a cold receptor reveals a general role for TRP channels in thermosensation, *Nature 416*, 52−58.
10. Gao, X., Wu, L., and O'Neil, R. G. (2003) Temperature-modulated diversity of TRPV4 channel gating: Activation by physical stresses and phorbol ester derivatives through protein kinase C-dependent and -independent pathways, *J. Biol. Chem. 278*, 27129−27137.

11. Benham, C. D., Davis, J. B., and Randall, A. D. (2002) Vanilloid and TRP channels: A family of lipid-gated cation channels, *Neuropharmacology 42*, 873−888.
12. Caterina, M. J., Schumacher, M. A., Tominaga, M., Rosen, T. A., Levine, J. D., and Julius, D. (1997) The capsaicin receptor: A heat-activated ion channel in the pain pathway, *Nature 389*, 816−824.
13. Tominaga, M., Caterina, M. J., Malmberg, A. B., Rosen, T. A., Gilbert, H., Skinner, K., Raumann, B. E., Basbaum, A. I., and Julius, D. (1998) The cloned capsaicin receptor integrates multiple pain-producing stimuli, *Neuron 21*, 531−543.
14. Ryu, S., Liu, B., and Qin, F. (2003) Low pH potentiates both capsaicin binding and channel gating of VR1 receptors, *J. Gen. Physiol. 122*, 45−61.
15. Prescott, E. D., and Julius, D. (2003) A modular PIP2 binding site as a determinant of capsaicin receptor sensitivity, *Science 300*, 1284−1288.
16. Jordt, S. E., and Julius, D. (2002) Molecular basis for species-specific sensitivity to "hot" chili peppers, *Cell 108*, 421−430.
17. Jordt, S. E., Tominaga, M., and Julius, D. (2000) Acid potentiation of the capsaicin receptor determined by a key extracellular site, *Proc. Natl. Acad. Sci. U.S.A. 97*, 8134−8139.
18. Jung, J., Hwang, S. W., Kwak, J., Lee, S. Y., Kang, C. J., Kim, W. B., Kim, D., and Oh, U. (1999) Capsaicin binds to the intracellular domain of the capsaicin-activated ion channel, *J. Neurosci. 19*, 529−538.
19. Caterina, M. J., Leffler, A., Malmberg, A. B., Martin, W. J., Trafton, J., Petersen-Zeitz, K. R., Koltzenburg, M., Basbaum, A. I., and Julius, D. (2000) Impaired nociception and pain sensation in mice lacking the capsaicin receptor, *Science 288*, 306−313.
20. Wahl, P., Foged, C., Tullin, S., and Thomsen, C. (2001) Iodo-resiniferatoxin, a new potent vanilloid receptor antagonist, *Mol. Pharmacol. 59*, 9−15.
21. Rigoni, M., Trevisani, M., Gazzieri, D., Nadaletto, R., Tognetto, M., Creminon, C., Davis, J. B., Campi, B., Amadesi, S., Geppetti, P., and Harrison, S. (2003) Neurogenic responses mediated by vanilloid receptor-1 (TRPV1) are blocked by the high affinity antagonist, iodo-resiniferatoxin, *Br. J. Pharmacol. 138*, 977−985.
22. Pomonis, J. D., Harrison, J. E., Mark, L., Bristol, D. R., Valenzano, K. J., and Walker, K. (2003) N-(4-tertiarybutylphenyl)-4-(3-cholorphyridin-2-yl)tetrahydropyrazine -1(2H)-carbox-amide (BCTC), a novel, orally effective vanilloid receptor 1 antagonist with analgesic properties: Ii. In vivo characterization in rat models of inflammatory and neuropathic pain, *J. Pharmacol. Exp. Ther. 306*, 387−393.
23. Walker, K. M., Urban, L., Medhurst, S. J., Patel, S., Panesar, M., Fox, A. J., and McIntyre, P. (2003) The VR1 antagonist capsazepine reverses mechanical hyperalgesia in models of inflammatory and neuropathic pain, *J. Pharmacol. Exp. Ther. 304*, 56−62.
24. Szallasi, A. (1994) The vanilloid (capsaicin) receptor: Receptor types and species differences, *Gen. Pharmacol. 25*, 223−243.
25. Witte, D. G., Cassar, S. C., Masters, J. N., Esbenshad, T., and Hancock, A. A. (2002) Use of fluorescent imaging plate reader-based calcium assay to assess pharmacological differences between the human and rat vanilloid receptor, *J. Biomol. Screening 7*, 466−475.
26. McIntyre, P., McLatchie, L. M., Chambers, A., Phillips, E., Clarke, M., Savidge, J., Toms, C., Peacock, M., Shah, K., Winter, J., Weerasakera, N., Webb, M., Rang, H. P., Bevan, S., and James, I. F. (2001) Pharmacological differences between the human and rat vanilloid receptor 1 (VR1), *Br. J. Pharmacol. 132*, 1084−1094.
27. Savidge, J., Davis, C., Shah, K., Colley, S., Phillips, E., Ranasinghe, S., Winter, J., Kotsonis, P., Rang, H., and McIntyre, P. (2002) Cloning and functional characterization of the guinea pig vanilloid receptor 1, *Neuropharmacology 43*, 450−456.
28. Seabrook, G. R., Sutton, K. G., Jarolimek, W., Hollingworth, G. J., Teague, S., Webb, J., Clark, N., Boyce, S., Kerby, J., Ali, Z., Chou, M., Middleton, R., Kaczorowski, G., and Jones, A. B. (2002) Functional properties of the high-affinity TRPV1 (VR1) vanilloid receptor antagonist (4-hydroxy-5-iodo-3-methoxyphenylacetate ester) iodo-resiniferatoxin, *J. Pharmacol. Exp. Ther. 303*, 1052−1060.
29. Szallasi, A., and Blumberg, P. M. (1990) Specific binding of resiniferatoxin, an ultrapotent capsaicin analog, by dorsal root ganglion membranes, *Brain Res. 524*, 106−111.
30. Szallasi, A., Blumberg, P. M., Annicelli, L. L., Krause, J. E., and Cortright, D. N. (1999) The cloned rat vanilloid receptor VR1 mediates both r-type binding and c-type calcium response in dorsal root ganglion neurons, *Mol. Pharmacol. 56*, 581−587.
31. Szallasi, A., Goso, C., Blumberg, P. M., and Manzini, S. (1993) Competitive inhibition by capsazepine of [3H]resiniferatoxin binding to central (spinal cord and dorsal root ganglia) and peripheral (urinary bladder and airways) vanilloid (capsaicin) receptors in the rat, *J. Pharmacol. Exp. Ther. 267*, 728−733.
32. Julius, D. J., Caterina, M. J., and Brake, A. J. (2002) Nucleic acid sequences encoding capsaicin receptor and uses thereof, U.S. Patent 6,335,180.
33. Szallasi, A., Lewin, N. A., and Blumberg, P. M. (1993) Vanilloid (capsaicin) receptor in the rat: Positive cooperativity of resiniferatoxin binding and its modulation by reduction and oxidation, *J. Pharmacol. Exp. Ther. 266*, 678−683.
34. Schmalhofer, W. A., Slaughter, R. S., Matyskiela, M., Felix, J. P., Tang, Y. S., Rupprecht, K., Kaczorowski, G. J., and Garcia, M. L. (2003) Di-substituted cyclohexyl derivatives bind to two identical sites with positive cooperativity on the voltage-gated potassium channel, K(v)1.3, *Biochemistry 42*, 4733−4743.
35. Acs, G., Lee, J., Marquez, V. E., and Blumberg, P. M. (1996) Distinct structure−activity relations for stimulation of 45Ca uptake and for high affinity binding in cultured rat dorsal root ganglion neurons and dorsal root ganglion membranes, *Brain Res. Mol. Brain Res. 35*, 173−182.
36. Gregoret, L. M., Rader, S. D., Fletterick, R. J., and Cohen, F. E. (1991) Hydrogen bonds involving sulfur atoms in proteins, *Proteins 9*, 99−107.
37. Iwaoka, M., Takemoto, S., and Tomoda, S. (2002) Statistical and theoretical investigations on the directionality of nonbonded S···O interactions. Implications for molecular design and protein engineering, *J. Am. Chem. Soc. 124*, 10613−10620.
38. Undem, B. J., and Kollarik, M. (2002) Characterization of the vanilloid receptor 1 antagonist iodo-resiniferatoxin on the afferent and efferent function of vagal sensory C-fibers, *J. Pharmacol. Exp. Ther. 303*, 716−722.
39. Hui, K., Liu, B., and Qin, F. (2003) Capsaicin activation of the pain receptor, VR1: Multiple open states from both partial and full binding, *Biophys. J. 84*, 2957−2968.
40. Jiang, Y., Ruta, V., Chen, J., Lee, A., and MacKinnon, R. (2003) The principle of gating charge movement in a voltage-dependent K^+ channel, *Nature 423*, 42−48.
41. Adolf, W., Sorg, B., Hergenhahn, M., and Hecker, E. (1982) Structure−activity relations of polyfunctional diterpenes of the daphnane type. I. Revised structure for resiniferatoxin and structure−activity relations of resiniferonol and some of its esters, *J. Nat. Prod. 45*, 347−354.
42. Walpole, C. S., Bevan, S., Bloomfield, G., Breckenridge, R., James, I. F., Ritchie, T., Szallasi, A., Winter, J., and Wrigglesworth, R. (1996) Similarities and differences in the structure−activity relationships of capsaicin and resiniferatoxin analogues, *J. Med. Chem. 39*, 2939−2952.
43. McDonnell, M. E., Zhang, S. P., Dubin, A. E., and Dax, S. L. (2002) Synthesis and in vitro evaluation of a novel iodinated resiniferatoxin derivative that is an agonist at the human vanilloid VR1 receptor, *Bioorg. Med. Chem. Lett. 12*, 1189−1192.
44. Appendino, G., Harrison, S., De Petrocellis, L., Daddario, N., Bianchi, F., Schiano Moriello, A., Trevisani, M., Benvenuti, F., Geppetti, P., and Di Marzo, V. (2003) Halogenation of a capsaicin analogue leads to novel vanilloid TRPV1 receptor antagonists, *Br. J. Pharmacol. 139*, 1417−1424.
45. Welch, J. M., Simon, S. A., and Reinhart, P. H. (2000) The activation mechanism of rat vanilloid receptor 1 by capsaicin involves the pore domain and differs from the activation by either acid or heat, *Proc. Natl. Acad. Sci. U.S.A. 97*, 13889−13894.
46. Kuzhikandathil, E. V., Wang, H., Szabo, T., Morozova, N., Blumberg, P. M., and Oxford, G. S. (2001) Functional analysis of capsaicin receptor (vanilloid receptor subtype 1) multimerization and agonist responsiveness using a dominant negative mutation, *J. Neurosci. 21*, 8697−8706.
47. Kolossvary, I., and Guida, W. C. (1999) Low-mode conformational search elucidated: Application to C39H80 and flexible docking of 9-deazaguanine inhibitors into PNP, *J.Comput. Chem. 20*, 1671−1684.

BI035981H